ENVIRONMENTAL RESEARCH
LETTERS

ACCEPTED MANUSCRIPT • OPEN ACCESS

Rise and fall of vegetation annual primary production resilience to climate variability projected by a large ensemble of Earth System Models' simulations

To cite this article before publication: Matteo Zampieri *et al* 2021 *Environ. Res. Lett.* in press https://doi.org/10.1088/1748-9326/ac2407

Rise and fall of vegetation annual primary production resilience to climate variability projected by a large ensemble of Earth System Models' simulations.

Matteo Zampieri[1*], Bruna Grizzetti[1], Andrea Toreti[1], Pierluca De Palma[2] and Alessio Collalti[3]

[1]European Commission - Joint Research Centre (JRC), Ispra IT

[2]Fincons SPA, Vimercate IT

[3]Institute for Agriculture and Forestry Systems in the Mediterranean, National Research Council of Italy (CNR-ISAFOM), Perugia (PG), Italy

*matteo.zampieri@ec.europa.eu

Abstract

Climate change is affecting natural ecosystems and society. Anticipating its impacts on vegetation resilience is critical to estimate the ecosystems' response to global changes and the reliability of the related ecosystem services, to support mitigation actions, and to define proper adaptation plans.

Here, we compute the Annual Production Resilience Indicator from gross primary production (GPP) data simulated by a large ensemble of state-of-the-art Earth System Models (ESMs) involved in the last Coupled Model Intercomparison Project (CMIP6) of the Intergovernmental Panel on Climate Change (IPCC).

In the *Sustainability (Taking the Green Road)* and *Middle of the Road* scenarios (ssp126 and ssp245), the areas where vegetation shows increasing GPP resilience are wider than the areas with decreasing resilience. The situation drastically reverses in the *Fossil-fuel Development (Taking the Highway)* scenario (ssp585). Among the larger countries, Brazil is exposed to the highest risk of experiencing years with anomalously low GPP, especially in the *Taking the Highway* scenario.

Social Media Abstract

Mitigating climate change favors vegetation resilience. Large regions will be at risk otherwise.

Introduction

The Sustainable Development Goals, formally embraced by the 2010 Conference of Parties, recognize the importance of ensuring conservation, restoration and sustainable use of terrestrial ecosystems and their services, and strengthening the resilience and adaptive capacity to climate-related hazards (SDG 15 and SDG 13, respectively; United Nations 2016). Stable ecosystems, characterized by small variations from their average state despite changes in environmental

conditions, are indeed considered healthy and reliable in terms of the services they provide (MAE 2005, Costanza et al. 2014). Ecosystems in good condition are necessary to secure the sustainability of human activities and human well-being (Maes et al., 2020).

The concept of resilience is closely connected to ecosystem stability. Resilience has been defined either as the larger disturbance that a system can absorb without losing its structure, relationships and functionalities (Holling 1973, 1996, Walker et al. 2004, Yi and Jackson 2021) or as the time required by an ecosystem to recover and return back to the equilibrium state after a disturbance (Pimm 1984, Yi and Jackson 2021). These definitions - termed 'ecological resilience' and 'engineering resilience', respectively - are conceptually clear but do not directly provide a practical way to measure resilience (Morecroft et al. 2012, Scheffer et al. 2015). In fact, a quantitative estimation of resilience requires objective methods to identify and measure the external stresses and shocks (Meyer 2016). Also as a result of such indeterminacy, a large number of indicators was proposed to measure different aspects of resilience (De Keersmaecker et al. 2014, Scheffer et al. 2015, Meyer 2016, Yi and Jackson 2021). Up to date, none of these methods has been used to evaluate vegetation resilience at the global level and in future climate scenarios yet.

Gross primary production (GPP) — the total carbon fixation by plants — is a primarily important terrestrial ecosystem function, at the point that it was also considered to be strongly related to resilience itself (Moore et al. 1993, Stone et al. 1996, Bryant et al. 2019). Climate change is indeed expected to alter vegetation GPP resilience by potentially compromising the availability of water for vegetation in dry regions (Santini et al. 2014, Zampieri et al. 2019) and in general by increasing the frequency, amplitude and duration of extreme events that are detrimental for vegetation productivity (Dosio et al. 2018, Naumann et al. 2018). At the same time, the increase of atmospheric CO_2 concentration coming along with global warming is expected to bring positive effects in terms of vegetation photosynthetic rate (although acclimation should be also considered) i.e. the so called 'CO_2 fertilization effect' (Sage and Kubian 2007) and water use efficiency (Peters et al. 2018).

Here, we used the Annual Production Resilience Indicator (R_p), defined as the squared mean annual GPP divided by its variance, which was recently proposed for a statistical evaluation of the production resilience of natural vegetation (Zampieri et al. 2019) and agricultural systems from annual production time-series (Zampieri et al. 2020b). R_p is a simple but powerful indicator with several interesting properties. Being inspired by the ecological definition of resilience, R_p is proportional to the amplitude of the largest disturbances that the system can absorb (measure by their rareness) and it is potentially consistent with the engineering definition (i.e. the return timing) as well (Zampieri 2021). It increases with diversity (number of species) and it accounts for memory effects, i.e., for perturbation recovery timings longer than a season (Zampieri et al. 2020b).

We compute the Annual Production Resilience Indicator from a new ensemble of about 480 Earth System Models (ESMs) simulations included in the Sixth Coupled Models Intercomparison Project (CMIP6, https://www.wcrp-climate.org/wgcm-cmip/wgcm-cmip6) of the Intergovernmental Panel on Climate Change (IPCC). ESMs are global climate models with an explicit representation of carbon processes and cycling over land, atmosphere and the oceans (Dahan 2010, Randall et al. 2019), allowing to explore future climate variability of vegetation GPP according to different greenhouse gases emission scenarios.

We quantify the relative changes in resilience of the GPP production with respect to period 1985-2015 for the near and far future periods (2021-2050 and 2051-2100) under three scenarios of socio-economical global changes, corresponding to different levels of greenhouse gases emissions and land-use (i.e., the *Sustainability*, the *Middle of the Road*, and the *Fossil-fuel Development* scenarios) and we compute country level statistics of the larger projected changes.

Data and Methods

The Annual Production Resilience Indicator (R_p), is based on two assumptions (Zampieri 2021). For annual producing systems such as agriculture or natural ecosystems that are sufficiently adapted to the environmental conditions and to the local climate, it is sensible to assume that the largest disturbances are rarer compared to the "normal" conditions (assumption 1) and that the largest disturbances result in larger impacts of the annual production values (assumption 2). Under such conditions, the size of the disturbance can be univocally measured by its rareness e.g. the return period of production anomalies (T*). Focusing on the production function only, the ecological resilience can be then simply measured by T^*_{MAX}, which is the return period of the largest adverse event that the system can cope with before losing completely the production ability. This approach is not sensitive to changes in composition and structure of the ecosystems, so it may allow for adaptation according to a more 'modern' interpretation of ecological resilience (Walker et al. 2004).

For homogeneous production systems, it can be demonstrated that T^*_{MAX} is proportional to the annual production resilience indicator, defined as:

$$(1)\quad R_p = \mu^2 / \sigma^2,$$

where μ is the mean and σ is the standard deviation of the annual production (see Appendix A). In case the annual production resilience indicator is evaluated over a region including bare ground, the indicator is sensitive to the vegetated portion only (Zampieri et al. 2019).

It is interesting and potentially useful to disentangle the effects of changes in the mean and in the variability of GPP on the annual production resilience indicator. This can be accomplished by approximating the R_P change with a first order 2D Taylor expansion of equation 1 as a function of the changes in the mean and in the standard deviation of GPP as follows:

$$(2)\quad R_{p\_s} = R_{p\_h} + \Delta R_p,$$

where the *s* stands for "scenario", the *h* stands for "historical", and Δ represents the difference between two periods.

$$(3)\quad \Delta R_p \simeq \partial R / \partial \mu \cdot \Delta \mu + \partial R / \partial \sigma \cdot \Delta \sigma$$

where ∂ is the partial derivative. By computing the derivatives and dividing both members of equation 3 by R_p one obtains:

$$(4)\quad \Delta R_p / R_p = 2\Delta\mu/\mu - 2\Delta\sigma/\sigma.$$

Thus, an indication on the changes induced by the mean and the variability on the production resilience may be obtained by comparing the projected relative changes of the mean and of the variability, using the same weight. Equation 4 provides a normalized indicator of such comparison:

$$(5)\quad (|\Delta\mu/\mu| - |\Delta\sigma/\sigma|) / (|\Delta\mu/\mu| + |\Delta\sigma/\sigma|),$$

which varies from -1 (variability dominates) to +1 (mean dominates), which is useful to assess and compare the dominant relative changes in different locations.

In this study, R_P and its changes are computed on a large ensemble composed of all the climate change simulations for vegetation gross primary production available from all the Earth System Grid Federation (ESGF) portals up to 31st December 2019. The full list of simulations is provided in Table 1, along with the detailed reference to the land surface component of the Earth System Models.

The ESMs land surface components include a prognostic representation of the biosphere with spatially distributed vegetation processes such as evapotranspiration, photosynthesis, carbon allocation and growth of leaves, stems and roots interacting with near surface meteorological variables such as temperature, radiation, wind and CO_2 concentration, and soil variables such as

moisture, carbon and nitrogen (see references in Table 1). Therefore, GPP variability in ESMs is the result of both bio–geophysical and bio–geochemical processes such as soil moisture dynamics and energy budget, permafrost thawing, atmospheric CO_2 fertilization and nitrogen limitation as well as land use changes defined as a function of the different future scenarios. Some of the models also include a simplified representation of abiotic stresses on vegetation, such as fires (Lawrence et al. 2019, Bastos et al. 2020).

Memory effects linked to antecedent drought conditions are well reproduced since soil moisture dynamics and the related physical feedbacks were quite well developed already in the GCMs (Seneviratne et al. 2010), which are the predecessors of the ESMs and from which ESMs inherits the representation of abiotic processes. In general, ESMs provide a reasonable representation of the GPP response to drought (see citations in Table 1), which is, however, largely variable among models (Knauer et al. 2015, Huang et al. 2016, Orth et al. 2020). This motivates the use of a large ensemble for a robust assessment of GPP changes such as the one used here.

The annual GPP is derived by summing up the monthly GPP outputs for each simulation listed in Table 1 consistently with the spatial variability of vegetation seasonality (Peano et al. 2019). The annual GPP data of each simulation is interpolated on a common 0.5 degrees regular grid with a second conservative remapping method (Jones 1999, Chen and Knutson 2008). The simulations' ensemble mean R_p is computed for each ESMs and for each period and scenario. Finally, the overall median of the R_P changes with respect to the historical period is computed for each future period and scenario. The robustness of the results is assessed by highlighting the areas where at least 75% of the models agree on the sign of changes.

Results

Future climate projections display significant changes of GPP variability resilience (Fig. 1) compared to period 1985-2014. The annual vegetation primary production resilience indicator is anticipated to generally increase in the lower emission scenarios (ssp126 and ssp245, Fig. 1 a,b,c, and d, respectively). The larger positive changes are expected to occur especially in the snow dominated bioclimatic regions (see Table S2). The amplitude and the area covered by these changes are comparatively larger in the ssp245 scenario than in the ssp126 scenario and increase with time towards the end of the 21st century (Table 2). Positive changes are also estimated for Central Africa and the Sahel regions, India and over the Himalayan Plateau. However, regions with loss of GPP resilience appear as well, especially in Brazil, China and surrounding countries of equatorial America. Under the ssp245 socio-economic scenario, the CMIP6 ESMs project resilience losses also in Mexico and the southern part of the US, the Mediterranean region, Southern Africa and Australia. This occurs not only in the far future (2051-2100, Fig. 1d), but also in the near future (2021-2050; Fig. 1c).

- Figure 1 -

Under moderate emission scenarios (ssp126 and ssp245), about one third of land area is going to experience an increase of vegetation annual GPP resilience over the period 2021-2050 (see Table 2). This proportion is slightly lower, about one forth, when considering only the areas where 75% of the models agree on the sign of changes. Differently, the area with positive changes will cover almost half of the global land area (less than one third when the constraint on models' agreement is introduced) over the period 2051-2100. Regions losing resilience cover a smaller percentage of the global area, about 10% under ssp245 in the near future period. The differences between the plain estimate and the one constrained on models' agreement become negligible for variations of resilience higher than 15% (Table 2).

The results for the ssp585 scenario stand out significantly compared to the lower emission scenarios. Broad areas with negative change (i.e. loss of vegetation GPP resilience) appear

already in the period 2021-2050 (Fig. 1e) in the Amazon region, the Unites States, South Canada, Western Europe, the Mediterranean basin, as well as in the Middle east, Central, Western and Southern Africa, Southeast Asia and China, and Oceania. Areas with at least 5% loss of vegetation GPP resilience are projected to cover approximately one fifth of the global land (12% considering models' agreement); while areas with more than 15% losses are projected to be limited to 3%. Positive gains of vegetation GPP resilience in boreal regions are simulated to be more limited with respect to the lower emission scenarios. Gains of at least 5% are expected to cover about one fourth of the global areas (15% considering models' agreement); while areas with changes larger than 15% are limited to the 6%, similarly to the ssp126 scenario.

The severity of the projected losses is expected to further exacerbate in the period 2051-2100. In the *Taking the Highway* scenario, less and less regions are expected to experience gains in vegetation GPP resilience. These regions are: La Plata basin in Argentina, part of the Sahel region, Eastern Africa, Western India, North-western China and some regions along the coast of the Arctic Sea. In general, areas gaining at least 5% resilience are simulated to be limited to 14% (8% considering model agreement) of global areas, while regions with more than 15% increase of vegetation primary production resilience are limited globally to 6% of the land area. The areas losing resilience are expected to outbalance those ones increasing resilience and cover 43% (25% considering models agreement) of global land area with more than 5% resilience losses. Globally, 13% of land areas are predicted to lose more than 15 % vegetation primary production resilience.

- Figure 2 -

The GPP resilience changes can be driven either by the change in the GPP mean and by the changes in the GPP variability due to climate change (see Methods). Positive resilience changes in the near future under moderate emission scenarios are often linked to positive changes in the mean annual GPP (Fig. 2a,b,c,d,e, S4) connected to overall higher levels of atmospheric CO_2 concentration and to higher mean growing temperature in Boreal Regions. Negative resilience changes are generally associated to an increase in the interannual variability of GPP (see Fig. S5). The areas affected by an increase of variability largely change across the scenarios and reach their maximum extent under the scenario ssp585 (Fig. 2e,f, S5e,f).

- Figure 3 -

Gain and losses of resilience are quantified at the national level in order to provide country-specific information for adaptation options, and possibly to support ambitious mitigation policies. This analysis is displayed in Figure 3 for the ten largest countries (and in Table S3 for all World countries). Russia is characterized by the widest gains of resilience, which could cover almost 70% of the country area in the period 2051-2100 under the ssp245 scenario. The spatial extent of areas expected to experience gains is reduced up to about 15% in the near future under the ssp585 scenario. This tendency continues towards the end of the century, under the ssp585 scenario, when also areas with GPP resilience losses start to appear. Canada shows a similar picture, but with less optimistic estimation of predicted losses largely outbalancing the gains in the 2051-2100 period under the ssp585 scenario. The US and China display similar figures, with gains predicted to reach 20% in the low emission scenarios (ssp126 and ssp245) and losses ranging from 10% to 15% in the ssp585 over the period 2051-2100. Among the largest countries, Brazil is the one characterized by the worst projections, with the risk of losing resilience in 50% of its total territory under the ssp585 scenario at the end of the 21st Century. It is worth noting that these changes are likely to represent an underestimation as the current trend of land-use change (Freitas et al. 2018) is only partially considered in the ESMs (Hurtt et al. 2020). Australia is estimated to undergo negligible losses, also because over desert and arid areas resilience changes are proportionally small. Nevertheless, Australia will experience comparatively large losses of resilience towards the end of the century under the ssp585 scenario. The European Union is characterized by a more stable situation with significant positive changes only under the ssp245 scenario over the period 2051-2100. India shows projections similar to the EU, but with significant areas of vegetation that

both gain and lose resilience under the high emission scenario at the end of the 21st Century. Large positive and negative changes in resilience are also estimated for Argentina under the high emission scenario (2051-2100). Whether or not these compensating changes in different area are beneficial for the countries' adaptive capacity could be subject of specific follow-up investigations.

Results for the remaining World countries (see Table S3) allow identifying severe cases, such as losses of resilience higher than 15% over more than 50% of the area under the ssp585 scenario over the period 2051-2100 in Gabon, Bhutan, Venezuela, Equatorial Guinea, Malaysia, Peru, Guyana, Lebanon, Japan, Congo, Bolivia, Honduras, Zambia, South Korea, Papua Nuova Guinea and other 16 countries. Under the same scenario, the list of 'winner' countries is much shorter, with only Somalia gaining at least 15% resilience over more than 50% of its territory. Countries having the largest benefit under the ssp245 scenario at the end of the century are Russia and the ones in Northern Europe. Under the ssp126 scenario, the benefits are geographically spread into more continents. In both ssp126 and ssp245 scenarios, there are almost no countries experiencing more than 15% losses of resilience over 10% of their land.

Discussion and Conclusions

This study implements a simple and robust statistical indicator, the Annual Production Resilience Indicator (R_p), able to provide bulk estimation of ecological resilience from annual production time-series. Being focused on production, R_p is not sensitive to changes in ecosystem structure and other state variables that play a fundamental part in Holling's definition of ecological resilience (Holling 1973). Conversely, it is formally consistent with more modern conception of resilience allowing adaptation and other changes in ecosystem structure in a resilience framework (Walker et al. 2004). Other indicators based on higher temporal resolution data could be employed as well in order to assess more detailed aspects of resilience in a non-linear dynamics framework (Yi and Jackson 2021). However, R_p already provides a quick and useful indication of the changes in statistical stability of the production time series in different periods, and it is especially suitable for being computed on large data volumes. Here, the vegetation GPP resilience changes are estimated with reference to the climate variability simulated by a large ensemble of state-of-the-art Earth System Models (ESMs).

While the main properties of R_p are already demonstrated (Zampieri et al. 2019, 2020b, Zampieri 2021), here we also present an interesting decomposition of the resilience changes in terms of the mean GPP and its variability. This assessment is potentially useful for adaptation planning that should presumably account differently for the changes in the mean with respect to the changes in variability of vegetation GPP in the future climate projections (MEARNS et al. 1997, Smit et al. 2000, van der Wiel and Bintanja 2021) . However, the implication of the estimated GPP resilience changes and of their drivers need to be interpreted and confirmed through dedicated local-scale assessments, also identifying the specific drivers of the changes. However, this needs to be discussed case by case as well. For instance, while gains in resilience could be generally considered a positive feature in dry environments, the implication in wet environment and over high latitudes should be further investigated considering more complex approaches (Drews and Greatbatch 2017, Laamrani et al. 2020).

Our results aim at providing a useful first-order indication that surely needs to be corroborated with further dedicated studies estimating also the specific drivers of resilience and accounting for the different natural and socio-economic perspectives. However, the analysis presented here is potentially very useful to identify the world regions where there might be losses of vegetation GPP resilience as well as the countries that are subject to the most urgent necessity of improving adaptive capacity and resilience to climate-related hazards under different future climate scenarios.

Our results show large differences in the changes of GPP resilience across the globe, depending on greenhouse gases concentration of the projected scenarios. Under low emission scenarios, as found in previous studies (Hubau et al. 2020), the CO_2 fertilization effect often prevail over the

negative effect due global warming (e.g. an increase in metabolic costs which in turn would lead to a reduction in forest productivity and their efficiency, (Collalti et al. 2020)) and to the increase of climate variability. These results are in general agreement with the observed changes in vegetation distribution that are already observed especially in boreal regions (Myneni et al. 1997). This tendency is expected to increase in the future climate scenarios, especially those with higher greenhouse gases and radiative forcing increases (Zampieri and Lionello 2010). However, radiation will always be a limiting factor for the vegetation adaptation at very high latitudes (Seddon et al. 2016).

The main findings point to areas in the mid-latitudes where vegetation resilience is estimated to decrease in the higher emission scenarios, such as the Mediterranean, the mid-West in the US, Central America, part of China, Southern Africa and Australia. This tendency might compromise the stability of agricultural production and the reliability of ecosystem services provided by the natural vegetation in these regions, unless sensible adaptation actions are taken. The relevance of mitigation is most evident under the higher emission scenarios, where vegetation resilience is affected in most land areas and especially in tropical regions, where society is highly dependent on ecosystem services and more vulnerable to climatic changes.

The results of our analysis strongly support the SDG-13 on taking action to combat climate change and its impacts. Over areas with a high level of anthropization, our results are relevant for agricultural production, which is a main source of employment, livelihood and income for a large portion of population especially in developing countries (SDG-1, no poverty) as well as a main food source (SDG-2, no hunger). Our results are also relevant for the SDG-15, on the sustainable management of ecosystems and halting land degradation and biodiversity loss.

Overall, in the scenario with lower mitigation (i.e. the *Fossil-fuel Development* scenario), the areas losing vegetation resilience are more than the ones gaining resilience, jeopardizing the stability of the ecosystems structure (and of the related services). Adapting to changes in variability more than to changes in the mean production of vegetation will be critical for society and natural ecosystems in areas experiencing vegetation GPP resilience losses.

Acknowledgments

For transparency and reproducibility, this paper uses publicly available data provided by the IPCC through the Earth System Grid Federation LLNL, CEDA, DKRZ, GFDL, IPSL, LIU, NCI and NCCS nodes (ESGF, https://esgf.llnl.gov/nodes.html) and open-source software to compute the annual production resilience indicator (Zampieri et al. 2020a).

Author Contributions: MZ conceived the study and drafted the paper, MZ and BG performed the analysis, PDP downloaded data and performed initial checking, all authors reviewed the manuscript and contributed to the final version.

Declaration of Interest statement: Authors declare no conflicts of interests.

References

Arora, V. K., and J. F. Scinocca. 2016. Constraining the strength of the terrestrial CO$_{2}$ fertilization effect in the Canadian Earth system model version 4.2 (CanESM4.2). Geoscientific Model Development 9:2357–2376.

Bastos, A., M. O'Sullivan, P. Ciais, D. Makowski, S. Sitch, P. Friedlingstein, F. Chevallier, C. Rödenbeck, J. Pongratz, I. T. Luijkx, P. K. Patra, P. Peylin, J. G. Canadell, R. Lauerwald, W.

Li, N. E. Smith, W. Peters, D. S. Goll, A. K. Jain, E. Kato, S. Lienert, D. L. Lombardozzi, V. Haverd, J. E. M. S. Nabel, B. Poulter, H. Tian, A. P. Walker, and S. Zaehle. 2020. Sources of Uncertainty in Regional and Global Terrestrial CO2 Exchange Estimates. Global Biogeochemical Cycles 34:e2019GB006393.

Bryant, T., K. Waring, A. Sánchez Meador, and J. B. Bradford. 2019. A Framework for Quantifying Resilience to Forest Disturbance. Frontiers in Forests and Global Change 2:56.

Chen, C.-T., and T. Knutson. 2008. On the Verification and Comparison of Extreme Rainfall Indices from Climate Models. Journal of Climate 21:1605–1621.

Chen, Y., J. Ryder, V. Bastrikov, M. J. McGrath, K. Naudts, J. Otto, C. Ottlé, P. Peylin, J. Polcher, A. Valade, A. Black, J. A. Elbers, E. Moors, T. Foken, E. van Gorsel, V. Haverd, B. Heinesch, F. Tiedemann, A. Knohl, S. Launiainen, D. Loustau, J. Ogée, T. Vessala, and S. Luyssaert. 2016. Evaluating the performance of land surface model ORCHIDEE-CAN~v1.0 on water and energy flux estimation with a single- and multi-layer energy budget scheme. Geoscientific Model Development 9:2951–2972.

Collalti, A., A. Ibrom, A. Stockmarr, A. Cescatti, R. Alkama, M. Fernández-Martínez, G. Matteucci, S. Sitch, P. Friedlingstein, P. Ciais, D. S. Goll, J. E. M. S. Nabel, J. Pongratz, A. Arneth, V. Haverd, and I. C. Prentice. 2020. Forest production efficiency increases with growth temperature. Nature Communications 11:5322.

Costanza, R., R. de Groot, P. Sutton, S. van der Ploeg, S. J. Anderson, I. Kubiszewski, S. Farber, and R. K. Turner. 2014. Changes in the global value of ecosystem services. Global Environmental Change 26:152–158.

Dahan, A. 2010. Putting the Earth System in a numerical box? The evolution from climate modeling toward global change. Studies in History and Philosophy of Science Part B: Studies in History and Philosophy of Modern Physics 41:282–292.

Dosio, A., L. Mentaschi, E. M. Fischer, and K. Wyser. 2018. Extreme heat waves under 1.5 and 2 degree global warming(Supplementary data). Environmental Research L:1–9.

Drews, A., and R. J. Greatbatch. 2017. Evolution of the Atlantic Multidecadal Variability in a Model with an Improved North Atlantic Current. Journal of Climate 30:5491–5512.

Forrest, M., H. Tost, J. Lelieveld, and T. Hickler. 2018. Towards an advanced atmospheric chemistry-enabled ESM with dynamic land surface processes: Part I - Linking LPJ-GUESS (v4.0) with EMAC modelling system (v2.53). Geoscientific Model Development Discussions 2018:1–21.

Freitas, F. L. M., G. Sparovek, G. Berndes, U. M. Persson, O. Englund, A. Barretto, and U. Mörtberg. 2018. Potential increase of legal deforestation in Brazilian Amazon after Forest Act revision. Nature Sustainability 1:665–670.

Garrigues, S., A. Olioso, J. C. Calvet, E. Martin, S. Lafont, S. Moulin, A. Chanzy, O. Marloie, S. Buis, V. Desfonds, N. Bertrand, and D. Renard. 2015a. Evaluation of land surface model simulations of evapotranspiration over a 12-year crop succession: impact of soil hydraulic and vegetation properties. Hydrology and Earth System Sciences 19:3109–3131.

Garrigues, S., A. Olioso, D. Carrer, B. Decharme, J.-C. Calvet, E. Martin, S. Moulin, and O. Marloie. 2015b. Impact of climate, vegetation, soil and crop management variables on multi-year ISBA-A-gs simulations of evapotranspiration over a Mediterranean crop site.

Geoscientific Model Development 8:3033–3053.

Gerber, S., L. O. Hedin, M. Oppenheimer, S. W. Pacala, and E. Shevliakova. 2010. Nitrogen cycling and feedbacks in a global dynamic land model. Global Biogeochemical Cycles 24.

Harper, A. B., P. M. Cox, P. Friedlingstein, A. J. Wiltshire, C. D. Jones, S. Sitch, L. M. Mercado, M. Groenendijk, E. Robertson, J. Kattge, G. Bönisch, O. K. Atkin, M. Bahn, J. Cornelissen, Ü. Niinemets, V. Onipchenko, J. Peñuelas, L. Poorter, P. B. Reich, N. A. Soudzilovskaia, and P. V Bodegom. 2016. Improved representation of plant functional types and physiology in the Joint UK Land Environment Simulator (JULES v4.2) using plant trait information. Geoscientific Model Development 9:2415–2440.

Holling, C. S. 1973. Resilience and stability of ecological systems. Annual Review of Ecology and Systematics 4:1–23.

Holling, C. S. 1996. Engineering Resilience versus Ecological Resilience. The National Academy of Sciences.

Huang, Y., S. Gerber, T. Huang, and J. W. Lichstein. 2016. Evaluating the drought response of CMIP5 models using global gross primary productivity, leaf area, precipitation, and soil moisture data. Global Biogeochemical Cycles 30:1827–1846.

Hubau, W., S. L. Lewis, O. L. Phillips, K. Affum-Baffoe, H. Beeckman, A. Cuní-Sanchez, A. K. Daniels, C. E. N. Ewango, S. Fauset, J. M. Mukinzi, D. Sheil, B. Sonké, M. J. P. Sullivan, T. C. H. Sunderland, H. Taedoumg, S. C. Thomas, L. J. T. White, K. A. Abernethy, S. Adu-Bredu, C. A. Amani, T. R. Baker, L. F. Banin, F. Baya, S. K. Begne, A. C. Bennett, F. Benedet, R. Bitariho, Y. E. Bocko, P. Boeckx, P. Boundja, R. J. W. Brienen, T. Brncic, E. Chezeaux, G. B. Chuyong, C. J. Clark, M. Collins, J. A. Comiskey, D. A. Coomes, G. C. Dargie, T. de Haulleville, M. N. D. Kamdem, J.-L. Doucet, A. Esquivel-Muelbert, T. R. Feldpausch, A. Fofanah, E. G. Foli, M. Gilpin, E. Gloor, C. Gonmadje, S. Gourlet-Fleury, J. S. Hall, A. C. Hamilton, D. J. Harris, T. B. Hart, M. B. N. Hockemba, A. Hladik, S. A. Ifo, K. J. Jeffery, T. Jucker, E. K. Yakusu, E. Kearsley, D. Kenfack, A. Koch, M. E. Leal, A. Levesley, J. A. Lindsell, J. Lisingo, G. Lopez-Gonzalez, J. C. Lovett, J.-R. Makana, Y. Malhi, A. R. Marshall, J. Martin, E. H. Martin, F. M. Mbayu, V. P. Medjibe, V. Mihindou, E. T. A. Mitchard, S. Moore, P. K. T. Munishi, N. N. Bengone, L. Ojo, F. E. Ondo, K. S.-H. Peh, G. C. Pickavance, A. D. Poulsen, J. R. Poulsen, L. Qie, J. Reitsma, F. Rovero, M. D. Swaine, J. Talbot, J. Taplin, D. M. Taylor, D. W. Thomas, B. Toirambe, J. T. Mukendi, D. Tuagben, P. M. Umunay, G. M. F. van der Heijden, H. Verbeeck, J. Vleminckx, S. Willcock, H. Wöll, J. T. Woods, and L. Zemagho. 2020. Asynchronous carbon sink saturation in African and Amazonian tropical forests. Nature 579:80–87.

Hurtt, G. C., L. Chini, R. Sahajpal, S. Frolking, B. L. Bodirsky, K. Calvin, J. C. Doelman, J. Fisk, S. Fujimori, K. K. Goldewijk, T. Hasegawa, P. Havlik, A. Heinimann, F. Humpenöder, J. Jungclaus, J. Kaplan, J. Kennedy, T. Kristzin, D. Lawrence, P. Lawrence, L. Ma, O. Mertz, J. Pongratz, A. Popp, B. Poulter, K. Riahi, E. Shevliakova, E. Stehfest, P. Thornton, F. N. Tubiello, D. P. van Vuuren, and X. Zhang. 2020. Harmonization of Global Land-Use Change and Management for the Period 850--2100 (LUH2) for CMIP6. Geoscientific Model Development Discussions 2020:1–65.

Ito, A., and M. Inatomi. 2011. Water-Use Efficiency of the Terrestrial Biosphere: A Model Analysis Focusing on Interactions between the Global Carbon and Water Cycles. Journal of Hydrometeorology 13:681–694.

Jones, P. W. 1999. First- and Second-Order Conservative Remapping Schemes for Grids in

Spherical Coordinates. Monthly Weather Review 127:2204–2210.

De Kauwe, M. G., J. Kala, Y.-S. Lin, A. J. Pitman, B. E. Medlyn, R. A. Duursma, G. Abramowitz, Y.-P. Wang, and D. G. Miralles. 2015. A test of an optimal stomatal conductance scheme within the CABLE land surface model. Geoscientific Model Development 8:431–452.

De Keersmaecker, W., S. Lhermitte, O. Honnay, J. Farifteh, B. Somers, and P. Coppin. 2014. How to measure ecosystem stability? An evaluation of the reliability of stability metrics based on remote sensing time series across the major global ecosystems. Global Change Biology 20:2149–2161.

Knauer, J., C. Werner, and S. Zaehle. 2015. Evaluating stomatal models and their atmospheric drought response in a land surface scheme: A multibiome analysis. Journal of Geophysical Research: Biogeosciences 120:1894–1911.

Laamrani, A., O. Valeria, A. Chehbouni, and Y. Bergeron. 2020. Analysis of the Effect of Climate Warming on Paludification Processes: Will Soil Conditions Limit the Adaptation of Northern Boreal Forests to Climate Change? A Synthesis.

Lawrence, D. M., R. A. Fisher, C. D. Koven, K. W. Oleson, S. C. Swenson, G. Bonan, N. Collier, B. Ghimire, L. van Kampenhout, D. Kennedy, E. Kluzek, P. J. Lawrence, F. Li, H. Li, D. Lombardozzi, W. J. Riley, W. J. Sacks, M. Shi, M. Vertenstein, W. R. Wieder, C. Xu, A. A. Ali, A. M. Badger, G. Bisht, M. van den Broeke, M. A. Brunke, S. P. Burns, J. Buzan, M. Clark, A. Craig, K. Dahlin, B. Drewniak, J. B. Fisher, M. Flanner, A. M. Fox, P. Gentine, F. Hoffman, G. Keppel-Aleks, R. Knox, S. Kumar, J. Lenaerts, L. R. Leung, W. H. Lipscomb, Y. Lu, A. Pandey, J. D. Pelletier, J. Perket, J. T. Randerson, D. M. Ricciuto, B. M. Sanderson, A. Slater, Z. M. Subin, J. Tang, R. Q. Thomas, M. Val Martin, and X. Zeng. 2019. The Community Land Model Version 5: Description of New Features, Benchmarking, and Impact of Forcing Uncertainty. Journal of Advances in Modeling Earth Systems 11:4245–4287.

MAE. 2005. Millennium Ecosystem Assessment. Ecosystems and Human Well-Being: Synthesis. Washington DC.

MEARNS, L. O., C. ROSENZWEIG, and R. GOLDBERG. 1997. MEAN AND VARIANCE CHANGE IN CLIMATE SCENARIOS: METHODS, AGRICULTURAL APPLICATIONS, AND MEASURES OF UNCERTAINTY. Climatic Change 35:367–396.

Meyer, K. 2016. A mathematical rewiew of resilience in ecology. Natural Resource Modeling 29:339–352.

Moore, J. C., P. C. de Ruiter, and H. W. Hunt. 1993. Influence of Productivity on the Stability of Real and Model Ecosystems. Science 261:906–908.

Morecroft, M. D., H. Q. P. Crick, S. J. Duffield, and N. A. Macgregor. 2012. Resilience to climate change: translating principles into practice. Journal of Applied Ecology 49:547–551.

Myneni, R. B., C. D. Keeling, C. J. Tucker, G. Asrar, and R. R. Nemani. 1997. Increased plant growth in the northern high latitudes from 1981 to 1991. Nature 386:698–702.

Naumann, G., L. Alfieri, K. Wyser, L. Mentaschi, R. A. Betts, H. Carrao, J. Spinoni, J. Vogt, and L. Feyen. 2018. Global Changes in Drought Conditions under Different Levels of Warming. Geophysical Research Letters.

Orth, R., G. Destouni, M. Jung, and M. Reichstein. 2020. Large-scale biospheric drought

response intensifies linearly with drought duration in arid regions. Biogeosciences 17:2647–2656.

Peano, D., S. Materia, A. Collalti, A. Alessandri, A. Anav, A. Bombelli, and S. Gualdi. 2019. Global Variability of Simulated and Observed Vegetation Growing Season. Journal of Geophysical Research: Biogeosciences 124:3569–3587.

Peters, W., I. R. van der Velde, E. van Schaik, J. B. Miller, P. Ciais, H. F. Duarte, I. T. van der Laan-Luijkx, M. K. van der Molen, M. Scholze, K. Schaefer, P. L. Vidale, A. Verhoef, D. Wårlind, D. Zhu, P. P. Tans, B. Vaughn, and J. W. C. White. 2018. Increased water-use efficiency and reduced CO(2) uptake by plants during droughts at a continental-scale. Nature geoscience 11:744–748.

Pimm, S. L. 1984. The complexity and stability of ecosystems. Nature 307:321–326.

Randall, D. A., C. M. Bitz, G. Danabasoglu, A. S. Denning, P. R. Gent, A. Gettelman, S. M. Griffies, P. Lynch, H. Morrison, R. Pincus, and J. Thuburn. 2019. 100 Years of Earth System Model Development. Meteorological Monographs 59:12.1-12.66.

Reick, C. H., T. Raddatz, V. Brovkin, and V. Gayler. 2013. Representation of natural and anthropogenic land cover change in MPI-ESM. Journal of Advances in Modeling Earth Systems 5:459–482.

Sage, R. F., and D. S. Kubian. 2007. The temperature response of C3 and C4 photosynthesis. Plant, Cell & Environment 30:1086–1106.

Santini, M., A. Collalti, and R. Valentini. 2014. Climate change impacts on vegetation andwater cycle in the Euro-Mediterranean region, studied by a likelihoodapproach. Regional Environmental Change 14:1405–1418.

Scheffer, M., S. R. Carpenter, V. Dakos, and E. H. van Nes. 2015. Generic Indicators of Ecological Resilience: Inferring the Chance of a Critical Transition. Annual Review of Ecology, Evolution, and Systematics 46:145–167.

Seddon, A. W. R., M. Macias-Fauria, P. R. Long, D. Benz, and K. J. Willis. 2016. Sensitivity of global terrestrial ecosystems to climate variability. Nature 531:229.

Seneviratne, S. I., T. Corti, E. L. Davin, M. Hirschi, E. B. Jaeger, I. Lehner, B. Orlowsky, and A. J. Teuling. 2010. Investigating soil moisture–climate interactions in a changing climate: A review. Earth-Science Reviews 99:125–161.

Smit, B., I. Burton, R. J. T. Klein, and J. Wandel. 2000. An Anatomy of Adaptation to Climate Change and Variability. Climatic Change 45:223–251.

Stone, L., A. Gabric, and T. Berman. 1996. Ecosystem Resilience, Stability, and Productivity: Seeking a Relationship. The American Naturalist 148:892–903.

United Nations. 2016. Report of the Inter-Agency and Expert Group on Sustainable Development Goal Indicators. New York.

Volodin, E. M., E. V Mortikov, S. V Kostrykin, V. Y. Galin, V. N. Lykossov, A. S. Gritsun, N. A. Diansky, A. V Gusev, and N. G. Iakovlev. 2017. Simulation of the present-day climate with the climate model INMCM5. Climate Dynamics 49:3715–3734.

Walker, B., C. S. Holling, S. R. Carpenter, and A. Kinzig. 2004. Resilience, adaptability and transformability in social-ecological systems. Conservation Ecology 9.

van der Wiel, K., and R. Bintanja. 2021. Contribution of climatic changes in mean and variability to monthly temperature and precipitation extremes. Communications Earth & Environment 2:1.

Yi, C., and N. Jackson. 2021. A review of measuring ecosystem resilience to disturbance. Environmental Research Letters 16:53008.

Zampieri, M. 2021. Reconciling the ecological and engineering definitions of resilience. Ecosphere.

Zampieri, M., B. Grizzetti, M. Meroni, E. Scoccimarro, A. Vrieling, G. Naumann, and A. Toreti. 2019. Annual Green Water Resources and Vegetation Resilience Indicators: Definitions, Mutual Relationships, and Future Climate Projections. Remote Sensing 11:2708.

Zampieri, M., and P. Lionello. 2010. Simple statistical approach for computing land cover types and potential natural vegetation. Climate Research 41.

Zampieri, M., A. Toreti, A. Ceglar, P. de Palma, and T. Chatzopoulos. 2020a. Analysing the resilience of the European commodity production system with PyResPro, the Python Production Resilience package.

Zampieri, M., C. J. Weissteiner, B. Grizzetti, A. Toreti, M. van den Berg, and F. Dentener. 2020b. Estimating resilience of crop production systems: From theory to practice. Science of The Total Environment 735:139378.

Figures and Tables

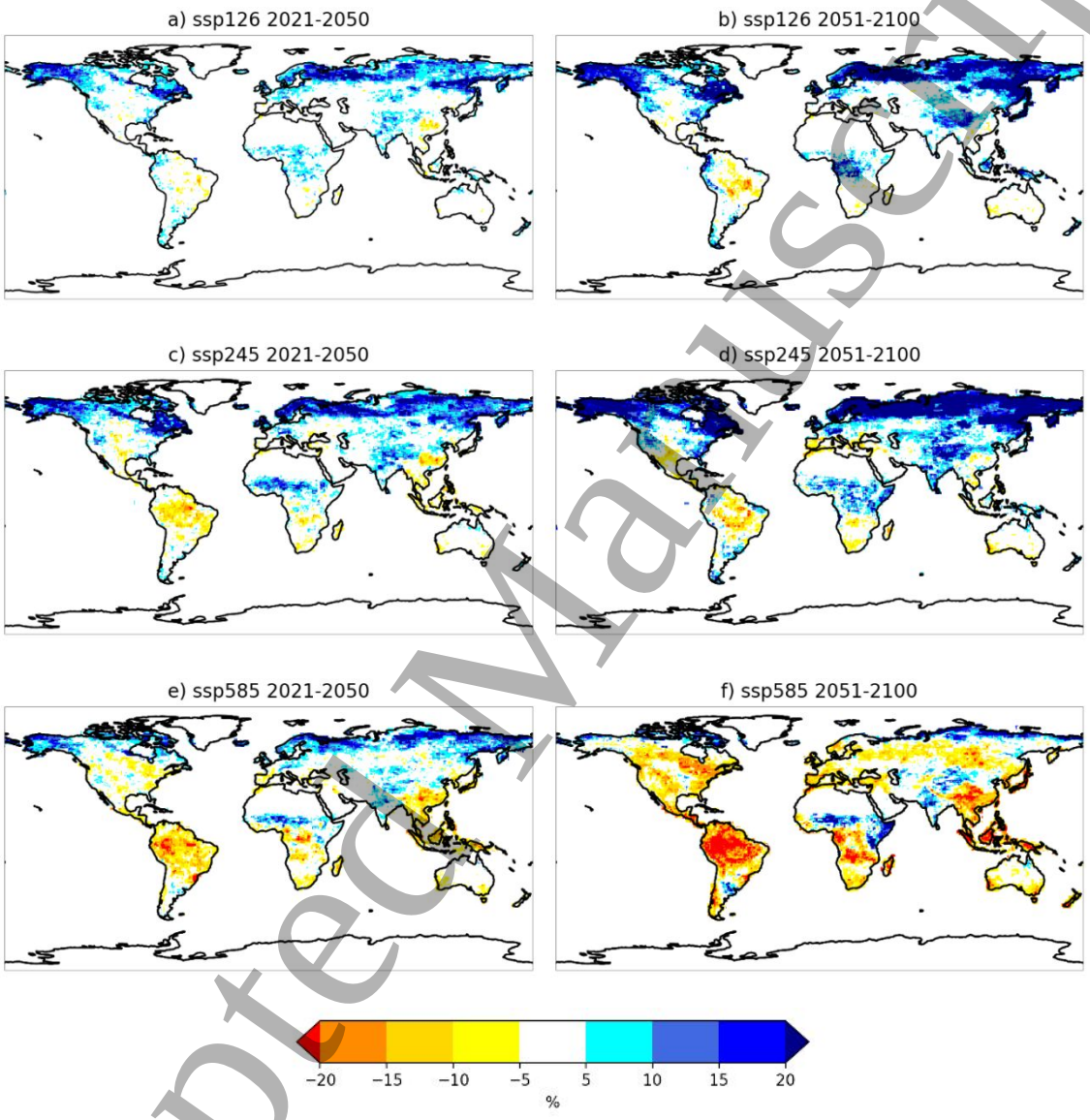

Figure 1. Global changes of annual gross primary production resilience (Rp) computed from an ensemble of 16 Earth System Models (ESMs) simulations under ssp126 (panels a and b), ssp245 (panels c and d), and ssp585 (panels e and f) CMIP6 scenarios in the periods 2021-2050 (panels a, c, and e) and 2051-2100 (panels b, d, and f) compared to the period 1985-2014.

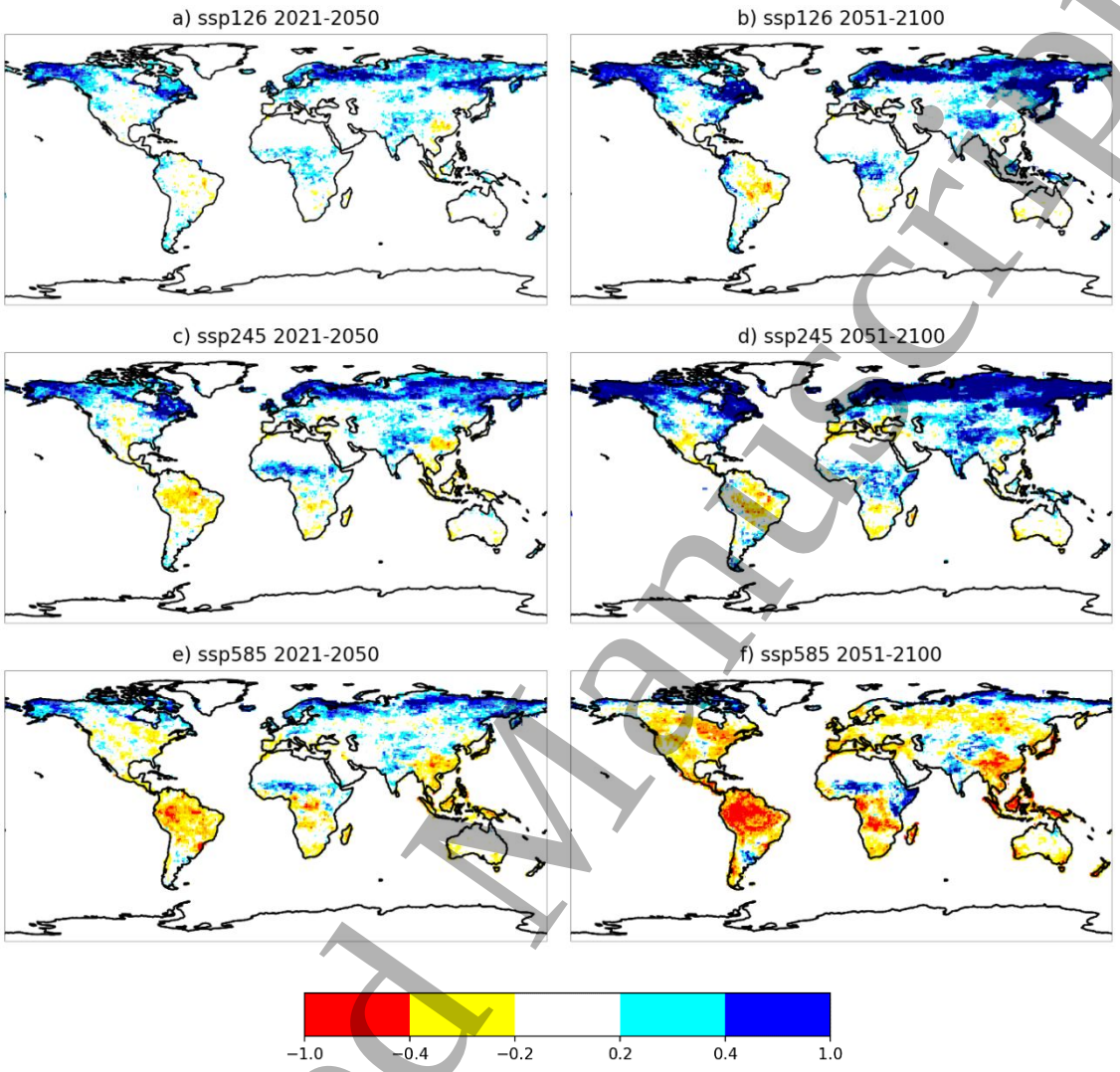

Figure 2. Ensemble mean share of the two factors triggering changes in the vegetation annual production resilience indicator (as from eq. 5, see Methods). Positive values (light and dark blue areas) point to changes in the resilience indicator mainly due to changes in the mean GPP. Negative values (red and yellow areas) are associated with grid points where the changes in the resilience indicator are mainly driven by changes in the GPP variability.

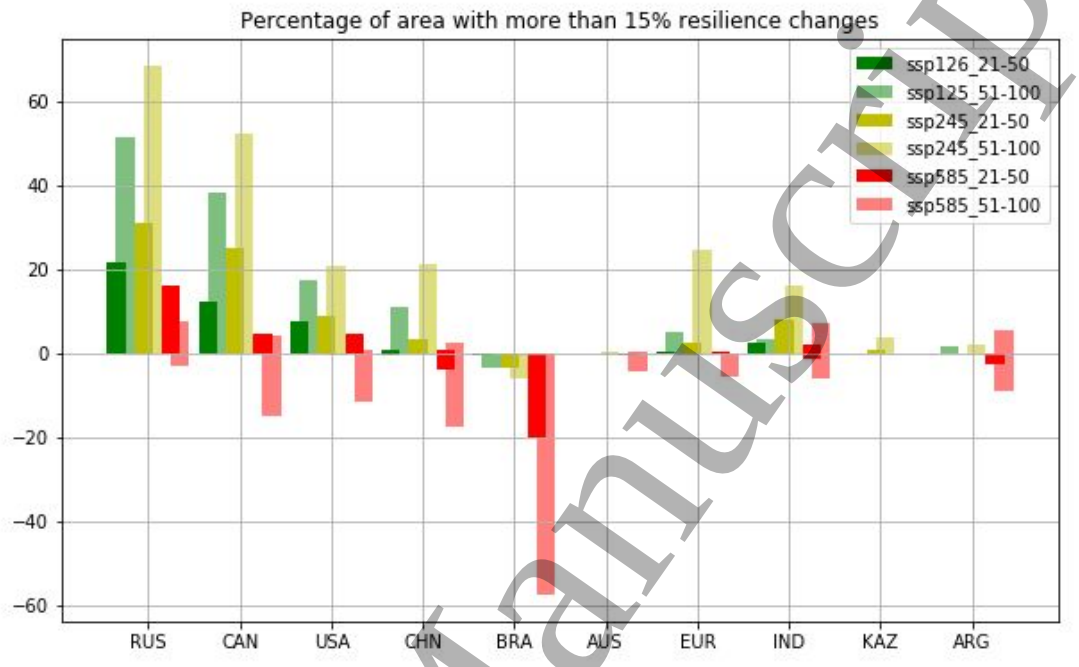

Figure 3. Percentages of area with more than 15% annual GPP resilience change for the ten wider countries, Russia (RUS), Canada (CAN), the United States of America (USA), China (CHN), Brazil (BRA), Australia (AUS), the European Union (EUR), India (IND), Kazakhstan (KAZ), and Argentina (ARG). Negative values refer to the percentage of areas with negative GPP resilience changes.

Table 1. Earth System Model (ESMs) simulations producing the annual gross primary production (GPP) data used in this study; with information on: modules delegated to the representation of land surface processes and GPP simulations (and associated reference publications); number of simulations available up to 31st December 2019 for the historical period and for ssp126, ssp245 and ssp585 future scenarios.

ESM	Land Model	historical	ssp126	ssp245	ssp585
ACCESS-ESM-5	CABLE w/Carbon cycle (De Kauwe et al. 2015)	1	1	1	1
CESM2-WACCM	CLM5 (Lawrence et al. 2019)	3	1	1	1
CESM2	CLM5 (Lawrence et al. 2019)	10	2	3	2
CNRM-CM6-1	ISBA with fixed LAI monthly climatology (Garrigues et al. 2015a, 2015b)	30	1	6	6
CNRM-ESM-1	ISBA with interactive LAI (Garrigues et al. 2015b, 2015a)	7	1	5	5
CanESM5-CanOE	CLASS-CTEM (Arora and Scinocca 2016)	3	3	3	3
CanESM5	CLASS-CTEM (Arora and Scinocca 2016)	50	50	50	50
EC-Earth3-Veg	LPJ-GUESS v4 (Forrest et al. 2018)	4	3	3	3
INM-CM4-8	no name (Volodin et al. 2017)	1	1	1	1
INM-CM5-0	no name[5]	10	1	1	1
IPSL-CM6A-LR	ORCHIDEE (Chen et al. 2016)	30	1	9	6
MIROC-ES2L	VISIT-e (Ito and Inatomi 2011)	3	1	1	1
MPI-ESM1-2-HR	JSBACH (Reick et al. 2013)	10	2	2	2
MPI-ESM2-2-LR	JSBACH (Reick et al. 2013)	10	10	10	10
NorESM2-LM	GFDL-LM3.0 (Gerber et al. 2010)	3	1	3	1
UKEMS1-0-LL	JULES (Harper et al. 2016)	19	5	4	5

Table 2. Fraction of global land area where the relative resilience indicator ($\Delta R_p/R_p$) exceeds different thresholds (5%; 10%; 15%; 20%) in the simulation ensemble median. The first estimation (third and fourth columns) considers all areas displaying changes larger than the thresholds. A second estimate (fifth and sixth columns) is restricted to the areas where at least the 75% of the models agree on the sign of changes.

		Fraction of land area with changing resilience		Fraction of land area considering 75% models' agreement	
Period	*Scenario*	*$\Delta R_p/R_p$>5%*	*$\Delta R_p/R_p$<5%*	*$\Delta R_p/R_p$>5%*	*$\Delta R_p/R_p$<5%*
2021-2050	ssp126	31%	2%	25%	1%
	ssp245	35%	9%	27%	4%
	ssp585	24%	21%	15%	12%
2051-2100	ssp126	41%	3%	36%	1%
	ssp245	48%	8%	27%	4%
	ssp585	14%	43%	8%	25%
		$\Delta R_p/R_p$>10%	$\Delta R_p/R_p$<10%	$\Delta R_p/R_p$>10%	$\Delta R_p/R_p$<10%
2021-2050	ssp126	15%	0%	13%	0%
	ssp245	21%	2%	19%	1%
	ssp585	12%	8%	9%	6%
2051-2100	ssp126	27%	0%	26%	0%
	ssp245	35%	2%	30%	1%
	ssp585	8%	27%	6%	20%
		$\Delta R_p/R_p$>15%	$\Delta R_p/R_p$<15%	$\Delta R_p/R_p$>15%	$\Delta R_p/R_p$<15%
2021-2050	ssp126	7%	0%	7%	0%
	ssp245	12%	0%	11%	0%
	ssp585	6%	3%	5%	2%
2051-2100	ssp126	20%	0%	19%	0%
	ssp245	26%	0%	25%	0%
	ssp585	5%	13%	4%	12%
		$\Delta R_p/R_p$>20%	$\Delta R_p/R_p$<20%	$\Delta R_p/R_p$>20%	$\Delta R_p/R_p$<20%
2021-2050	ssp126	3%	0%	3%	0%
	ssp245	6%	0%	6%	0%
	ssp585	3%	0%	2%	0%
2051-2100	ssp126	14%	0%	14%	0%
	ssp245	20%	0%	20%	0%
	ssp585	3%	6%	2%	5%